Photoinduced structural phase transitions and their dynamics

2001 J. Phys.: Condens. Matter 13 R693

(http://iopscience.iop.org/0953-8984/13/35/201)

INSTITUTE OF PHYSICS PUBLISHING JOURNAL OF PHYSICS: CONDENSED MATTER

J. Phys.: Condens. Matter **13** (2001) R693–R721 PII: S0953-8984(01)23954-X

TOPICAL REVIEW

Photoinduced structural phase transitions and their dynamics

Keiichiro Nasu, Huai Ping and Hideo Mizouchi

Solid State Theory Division, Institute of Materials Structure Science, KEK,
Graduate University for Advanced Study, 1-1 Oho, Tsukuba, Ibaraki 305-0801, Japan

E-mail: knasu@post.kek.jp

Received 4 June 2001, in final form 4 June 2001
Published 16 August 2001
Online at stacks.iop.org/JPhysCM/13/R693

Abstract

A general concept for photoinduced structural phase transitions is developed, in terms of the hidden multi-stability of the ground state and the proliferations of optically excited states. Taking the ionic (I) to neutral (N) phase transition in the organic charge transfer (CT) crystal, tetrathiafuluvalene-p-chloranil, as a typical example for this type of transition, we, at first theoretically show an adiabatic path which starts from CT excitons in the I-phase, but finally reaches to a N-domain with a macroscopic size. In connection with this I–N transition, the concept of the initial condition sensitivity is also developed so as to clarify experimentally observed nonlinear characteristics of this material.

Then, using a simplified model for the many-exciton system, we theoretically study the early-time quantum dynamics of the exciton proliferation, which finally results in the formation of a domain with a large number of excitons. For this purpose, we derive a stepwise iterative equation to describe the exciton proliferation, and clarify the origin of the initial condition sensitivity.

Possible differences between a photoinduced non-equilibrium phase and an equilibrium phase at high temperatures are also clarified from general and conceptional points of view, in connection with recent experiments on the photoinduced phase transition in an organo-metallic complex crystal. It will be shown that the photoinduced phase can make a new interaction appear as a broken symmetry only in this phase, even when this interaction is almost completely hidden in all the equilibrium phases, such as the ground state and other high-temperature phases.

(Some figures in this article are in colour only in the electronic version; see `www.iop.org`)

1. Introduction

There are various kinds of materials around us, and they are such ones that few kinds of macroscopic numbers of atoms or molecules are condensed with a definite composition ratio. Without changing this chemical composition, a material can take various phases from gaseous and liquid phases to crystalline ones, as temperature decreases. Even at low temperatures, a material can take various crystalline phases, whose crystal structure and electronic state change as temperature decreases. However, all these states are so-called equilibrium phases, in the sense that the free energy of each state takes its global minimum at each temperature.

Let us now proceed to non-equilibrium phases generated from an equilibrium one by some external stimulation or excitation. Usually, these states are transient ones having higher energies than the equilibrium one, but, depending on the type of stimulation or excitation, we may get a variety of states, even if the starting equilibrium phase is the same. They relax down to the starting equilibrium after a period of time. However, if they are a locally stable state, in the sense that their free energy take local minima separated from the global one by substantial energy barriers, the time required for relaxation will be long. In that case, we can complete the necessary observations to determine their characteristics within this long lifetime. Hence, such a long-lived locally stable non-equilibrium phase is effectively the same as the equilibrium one.

Various amorphous crystals are well known as typical examples for these non-equilibrium phases. They are brought about by cooling materials rapidly from their high-temperature phases. The lifetime of the relaxation is believed to be much longer than the time scale of our daily life. Unfortunately, however, these amorphous crystals have no well defined long-range periodic crystalline or electronic order.

Very recently, a new class of insulating solids has been discovered, which, when illuminated by only a few visible photons, become pregnant with a macroscopic excited domain that has new structural and electronic orders quite different from the initial ground state (equilibrium phase). This phenomenon is called 'photoinduced phase transition' and we can generate new long-lived locally stable macroscopic non-equilibrium phases through the excitations (or stimulations) by a few visible photons. The purpose of this paper is to review recent theoretical and experimental studies on this phenomenon.

2. Relaxation of optically excited states and photoinduced structural phase transitions

As is already well known, an electron in an insulating crystal induces a local lattice distortion around itself, when it is excited by a photon. This phenomenon is called the 'lattice relaxation' of an optical excitation, and the resultant state is often called the 'photoinduced structural change', as schematically shown in figure 1. This relaxation phenomenon has been studied in detail, in various kinds of insulating crystals, during the last 50 years. According to the original concept of this lattice relaxation, however, it is tacitly assumed to be a microscopic phenomenon, in which only few atoms and electrons are involved [1].

In recent years, on the other hand, there have been discovered many unconventionally photoactive solids, where the relaxation of optical excited states results in various collective motions involving a large number of atoms and electrons. In some cases, it results in a macroscopic excited domain with new structural and electronic orders quite different from the original ones. This situation can be called 'photoinduced structural phase transition (PSPT)' [2].

These problems are closely related to the hidden multi-stability intrinsic to each solid. If the ground state of a solid is pseudo-degenerate, being composed of true and false ground

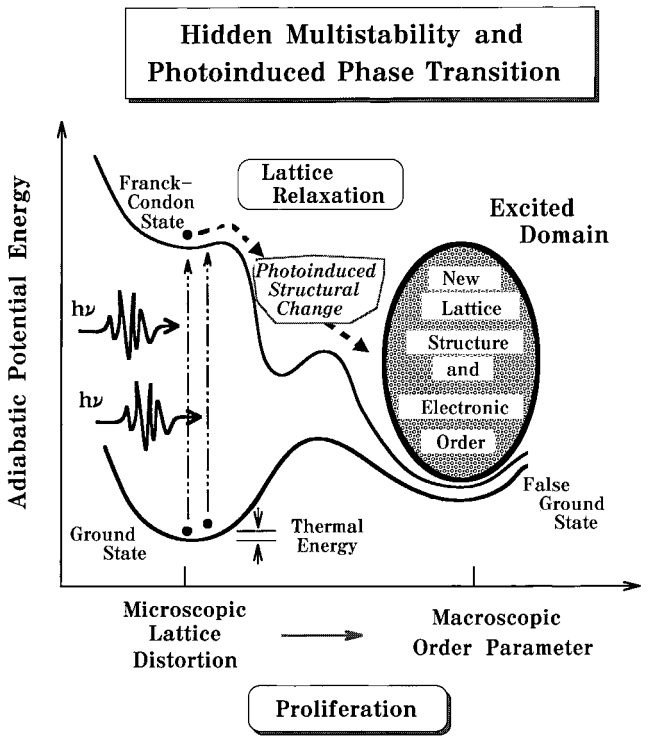

Figure 1. Schematic illustration of photoinduced structural phase transition, hidden multi-stability, proliferation and thermal energy.

states with each structural and electronic orders different from others, we call it multi-stable. In this case, the photo-absorption, being initially a single-electron excitation from the true ground state, can trigger local but macroscopic instabilities. The photo-absorption can induce low-lying collective excitations during the lattice relaxation, and can finally produce a false ground state at the expense to create boundaries between the two states. Thus a local but macroscopic excited domain appears. In other words, the initially created single-electron excitation proliferates during the relaxation, and grows up into a macroscopic order, as schematically shown in figure 1.

The origin of the pseudo-degeneracy can be understood from the conceptional point of view related with the cohesive mechanism of each solid. As mentioned before, the solid is composed of macroscopic numbers of few kinds of atoms or molecules with a definite composition ratio. However, even if the constituent atoms (molecules) are defined, the structural and electronic orders, which will be realized in the macroscopic ground state, are not always determined straightforwardly. For example, in the case of alkali halide, the ionic state and the covalent one are two well known candidates for the ground state [3]. Moreover, if there are two predominant but mutually conflicting elements in the original Hamiltonian, there appear two candidates that inherit this conflict. Thus, it is quite usual that we have the multi-stability or the pseudo-degeneracy with the true and false ground states.

It is also very important to see the relation between photoinduced phase transitions and the ordinary ones due to the thermal excitation. When the false ground state is just above the true one, and easily excited by the thermal energy, we may get the ordinary phase transition, and can

recognize the presence of this false ground state. However, there will be various other cases that the energy of the false ground state is too high to be excited thermally. Ordinary thermodynamic measurements are concerned only with the true ground state or small excitations therefrom, and hence can never detect such hidden states. Even in these difficult cases, we can create the false ground state by the photo-excitation and the lattice relaxation therefrom, as schematically shown in figure 1.

Such a false ground state always disappears finally within a finite lifetime, and can never be permanent, as mentioned before. However, according to the recent progress of laser spectroscopy techniques, an infinite lifetime is no longer necessary for a state to be recognized as a well-defined state, provided that it can last long enough to be clearly observed by other photons to detect it.

Let us briefly consider the difference between the present photoinduced phase transition and the so-called 'new material design (or search)', which is the latest trend in the field of the material science. One of the standard techniques for the new material design (or search) is to apply static external fields such as magnetic fields or pressures onto a material, which is expected to give novel or anomalous properties absent in other materials existing already. Another standard technique is to design or synthesize the material by changing its chemical composition, little by little, so that it will show quite new properties.

In the case of static external field, however, this changes all the electronic states of the material, both ground and excited states, unselectively. Photons have definite momentum, phase, helicity and energy, and hence, they can create only particular excited states, selectively and quite intensively. In contrast to the chemical design or synthesis, the photoinduced phase transition does not change the chemical composition of the material, but can realize new states. Thus the research for photoinduced phase transitions will be able to open a new multistoried concept for materials.

3. Photoinduced ionic–neutral phase transition in organic molecular crystal TTF-CA

As one of the typical examples for the PSPT, here we will be concerned with the photoinduced I–N transition in an organic molecular crystal tetrathiafuluvalene-p-chloranil (TTF-CA), and review the present stage for its experimental studies. Both tetrathiafuluvalene (TTF) and p-chloranil (CA) are planar organic molecules (figure 2(a)), and their crystal has a quasi-1D chain-like structure, in which these two molecules are alternately stacked, along this 1D chain axis.

In the true ground state of this crystal at absolute zero of temperature, TTF and CA become a cation and an anion, respectively, and make a dimer with each other as shown in figure 2(a). This is called the I-phase. On the other hand, we also have the N-phase, in which neutral TTF and CA are stacked alternately without dimerization (figure 2(d)). This is the accidentally pseudo-degenerate false ground state. At absolute zero of temperature, it is just above the ionic true ground state.

It is now well established that, keeping this material in the low enough temperature, but shining a strong laser light of about 0.6–2.2 eV onto it, we can generate the N-domain even in the ionic ground state, as shown in figure 2(c). This change was confirmed by the change of the optical reflectance spectrum. In fact, as the N-domain expands in the I-phase, a new peak appears at around 3 eV in that spectrum. This N-domain is composed of about 200–1000 neutral pairs, and can last for about 10^{-3} s [4]. This is nothing else but the PSPT. We can think of a simple and intuitive scenario for this transition in such a way as schematically shown in figures 2(b) and 2(c). That is, a single photon can make a single charge transfer (CT) excitation between neighbouring molecules, which is just equal to a neutral pair, and after

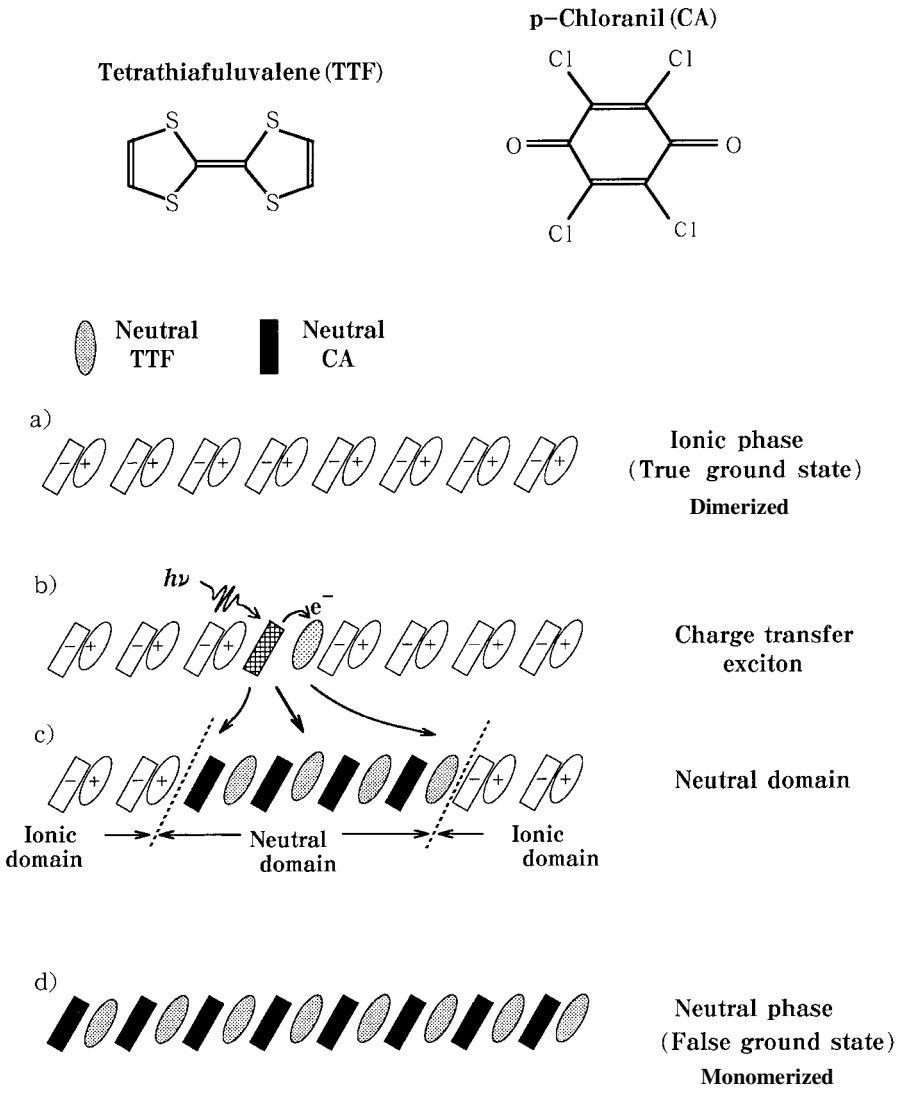

Figure 2. Schematic illustration of photoinduced ionic → neutral structural phase transition in TTF-CA crystal. (a) Ionic phase, (b) charge transfer exciton, (c) neutral domain, (d) neutral phase.

that, the number of this neutral pair will increase like a domino game. However, by the recent experimental studies shown in figure 3 [5], this simple scenario is proved wrong.

In this figure, we have shown the photo-absorption spectrum of TTF-CA as a small inset. It has two peaks at 0.6 and 2.2 eV. The first one, being the elementary optical excitation of this crystal, corresponds to the aforementioned inter-molecular CT excitation. Among a macroscopic number of neighbouring ion pairs (TTF^+ and CA^-) in figure 2(a), only a single neighbouring ion pair returns back to a neutral pair (TTF and CA) by this excitation as shown in figure 2(b), and this neutral pair also itinerates along the crystal axis, keeping all other pairs still ionic. This is nothing else but the so-called inter-molecular CT exciton, wherein a hole and an electron (a positive charge and a negative one relative to the I-phase) are bound together,

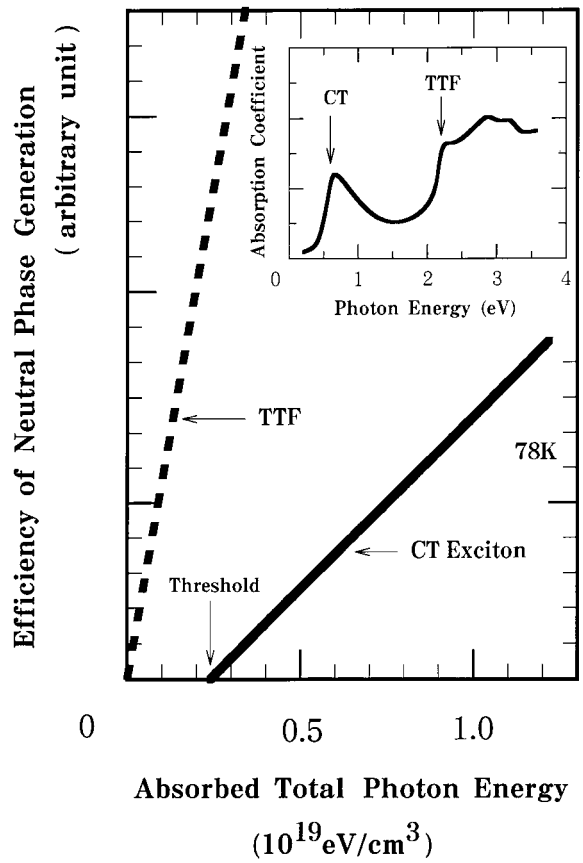

Figure 3. The efficiency of neutral phase generation in TTF-CA as a function of total absorbed photonic energy. The small inset denotes the light absorption spectrum of TTF-CA crystal. From Tanimura [5].

so that they are always at two neighbouring molecules even if their centre of mass itinerates. The second peak at 2.2 eV corresponds to an intra-molecular electronic transition of TTF. The thick solid line in figure 3 denotes the efficiency of the N-phase generation as function of the exciting photon intensity, when the photon energy is fixed at this CT exciton (0.6 eV). We can clearly see that there is a threshold in the intensity below which the N-phase can never be generated. This means that a single CT exciton alone can never result in the N-phase, but only through a nonlinear co-operation between several photo-excited CT excitons can the new phase be attained. This is the first noteworthy characteristic of the TTF-CA crystal.

4. Initial condition sensitivity

The second noteworthy characteristic, which we can see from figure 3, is the difference between the dashed line and the aforementioned thick solid line. Exactly speaking, the horizontal axis of this figure does not simply denote the photon intensity itself, but denotes the total photon energy which is absorbed in the unit volume of the TTF-CA crystal. This total energy is calculated by taking three quantities into account; the absorption coefficient, the energy of the photon and its intensity. Thus, we can compare the 0.6 eV excitation and the 2.2 eV excitation

(the thick dashed line) on an equal footing. For example, if we focus on the point with a value 0.25 of the horizontal axis in figure 3, we find that the efficiency becomes very high or almost zero, depending sensitively on the photon energy, although the total absorbed photonic energies are the same. We can also excite using various other photons in between (0.6–2.2 eV), keeping the total absorbed photonic energies the same. However, all these excitations give different efficiencies, ranging between the two lines in figure 3.

From this fact, we can immediately conclude that this is not an ordinary thermal phase transition. In the experimental studies for photoinduced phase transitions, the first thing we have to examine is whether it is an ordinary thermal phase transition or not, because the absorbed photons may often be converted into heat in the crystal, raising up its temperature, and may indirectly result in ordinary thermal phase transitions. In the case of this indirect thermal phase transition, however, its generation efficiency will depend only on the total absorbed photon energy, and will never sensitively depend on the type of excitation. Figure 3 shows that the generation efficiency quite sensitively depends on the type of excitation, that is the exciting photon energy, even if the total absorbed photonic energies are the same. In figure 1, the aforementioned two types of excitation start from the common ground state minimum equally, and moreover, the energies of the final states of the Franck–Condon transition are almost the same.

Here, we should emphasize the so-called Franck–Condon principle. The optical transition can complete within a time of the order of 10^{-15} s, provided that its transition energy is in the visible region. But the period of oscillation of a crystal lattice or phonon is of the order of 10^{-12} s. Thus, the configuration of the crystal lattice can never change during the optical transition and, hence, it can occur only vertically, as schematically shown in figure 1. Consequently, possible differences between the aforementioned two transitions are only in the electronic natures of these Franck–Condon-type excited states, from which the lattice relaxation and the proliferation start. However, this small difference in the initial state of the relaxation afterwards diverges and finally determines the occurrence or non-occurrence of the photoinduced phase transition. This is the so-called 'initial condition sensitivity', peculiar to the dynamics of nonlinear systems.

As is well known, the initial condition sensitivity has been studied mainly from the mathematical point of view, by taking classical nonlinear model systems with only a few degree of freedoms [6]. The setting up of the initial condition, in this case, is also a purely mathematical and artificial procedure in order to solve nonlinear differential equations that describe these model systems. On the other hand, the present case is the formation of a macroscopic order in a real material, and the setting up of the initial condition itself is also a real physical process. As mentioned before, it is set by choosing the spatiotemporal pattern of the exciting photon pulse and, hence, it is in compliance with the quantum uncertainty. Thus, the studies for the photoinduced phase transitions will open new aspects of the nonlinear dynamics and self-organization phenomena.

5. Adiabatic path of photoinduced ionic–neutral phase transition in TTF-CA crystal

Keeping these points in mind we have, very recently, theoretically clarified the adiabatic relaxation path, which starts from a Franck–Condon-type optical excitation in the ionic ground state of the TTF-CA crystal, and terminates up to the large N-domain formation in this crystal [7].

Let us review this in detail. In order to clarify the photoinduced phenomena in TTF-CA theoretically, we have to specify our microscopic model to describe the many-electron system strongly coupling with lattice distortions (phonons) in this molecular crystal. The constituent

TTF and CA molecules are, of course, originally neutral. However, when they are condensed as a crystal at low enough temperatures below 84 K, the whole system becomes the ionic and dimerized phase shown in figure 2(a). At temperatures higher than 84 K, it returns to the neutral and monomeric phase as shown in figure 2(d), and this ordinary thermal phase transition is the first-order one [8].

As shown by Soos theoretically [9], the change from the original neutral state to the ionic one can be described as an electron transfer from the highest occupied molecular orbital (HOMO) of TTF to the lowest unoccupied molecular orbital (LUMO) of CA. The main energy gain in the ionic state relative to the neutral one is the long-range Coulomb interaction between electrons and ions, in particular the Coulomb attraction between a cation and an anion thus generated, and this energy gain increases if the inter-molecular distance decreases after the ionization, as shown by Sakano and Toyozawa [10].

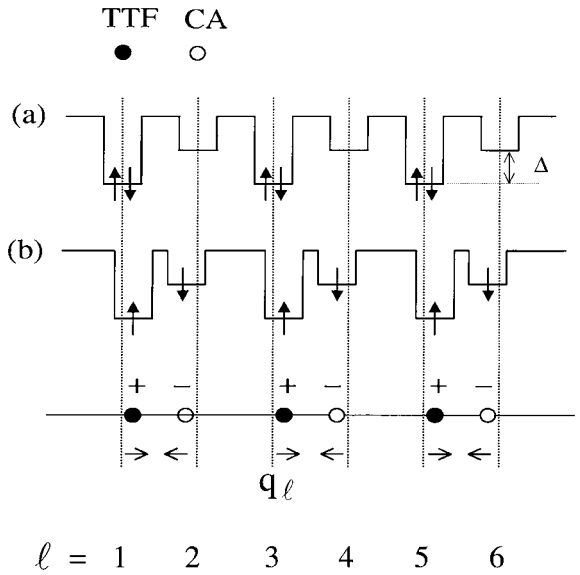

Figure 4. Schematic illustration of (a) neutral and (b) ionic phases in TTF-CA crystal. Up and down arrows denote the electrons and their spins. Δ denotes the energy difference between the HOMO and the LUMO. q_ℓ is the displacement of the molecule at that site.

5.1. Model Hamiltonian

Our theory is intended to take these essential points into account directly, and is based on the extended Peierls–Hubbard model for valence electrons in the HOMO of TTF molecules and the LUMO of CA molecules as schematically shown in figure 4 [7]. The inter-molecular Coulomb repulsion in this model is assumed to depend nonlinearly on the inter-molecular distance. This model also takes weak interactions between 1D chains into account, so that we can describe the N-domain formation in the three-dimensional TTF-CA crystal more realistically. Our Hamiltonian reads

$$H = H_{el} + H_{ph} + H_{inter} \tag{1}$$

where H_{el}, H_{ph} and H_{inter} denote the Hamiltonians of the electron part, the phonon part and the inter-chain interaction. The electronic part H_{el} is given as

$$H_{el} \equiv -T_i \sum_{\ell,\sigma}[(C^+_{\ell,\sigma}C_{\ell+1,\sigma}) + \text{HC}] + \frac{\Delta}{2}\sum_{\ell}(-1)^{\ell}n_{\ell} + U\sum_{\ell} n_{\ell,\alpha}n_{\ell,\beta} - \sum_{\ell\in\text{odd}} V_{\ell}(q_{\ell}, q_{\ell+1})[2 - n_{\ell}]n_{\ell+1} - \sum_{\ell\in\text{even}} V_{\ell}(q_{\ell}, q_{\ell+1})[2 - n_{\ell+1}]n_{\ell} \tag{2}$$

$$n_{\ell,\sigma} \equiv C^+_{\ell,\sigma}C_{\ell,\sigma} \qquad n_{\ell} \equiv \sum_{\sigma} n_{\ell,\sigma} \tag{3}$$

where T_i is the transfer energy of an electron between a HOMO and its neighbouring LUMO. $C^+_{\ell,\sigma}$ is the creation operator of an electron with spin σ at the ℓth lattice site, which is numbered from left to right along the 1D chain as shown in figure 4: odd sites correspond to the HOMO, while the even ones correspond to the LUMO. Δ in (2) is the energy difference between the HOMO and the LUMO, while U is the intra-molecular Coulomb repulsive energy of electrons, and is assumed to be common to both the HOMO and the LUMO. V_{ℓ} in (2) is the Coulomb interaction between two neighbouring molecules, wherein the total charge in the TTF site ($\ell \in$ odd) is $+[2 - n_{\ell}]$, while that in the CA site ($\ell \in$ even) is $-n_{\ell}$. As mentioned before, this interaction is assumed to depend nonlinearly on the change of the inter-molecular distance $(q_{\ell} - q_{\ell+1})$, where q_{ℓ} is the displacement of each molecule along the chain axis as shown in figure 4. The unit of length is the original inter-molecular distance. Thus, V_{ℓ} is given as

$$V_{\ell}(q_{\ell}, q_{\ell+1}) = V_0 + \beta_1(q_{\ell} - q_{\ell+1}) + \beta_2(q_{\ell} - q_{\ell+1})^2 \tag{4}$$

where V_0 is the original value of V_{ℓ}, while β_1 and β_2 are its first- and second-order expanding coefficients with respect to $(q_{\ell} - q_{\ell+1})$.

It is well known that the electron–phonon coupling leading to the dimerization may have two origins. The first one is the present case shown in (4), being the modulation of V_{ℓ}: this model was first proposed by Sakono and Toyozawa [10]. The second one is the modulation of T_i [11–13]. Because of the small overlap between the HOMO and the LUMO, this T_i becomes so small that its distance variation can be neglected. Moreover, as we will show later, our model is rather straightforward to make the N–I phase transition a first-order one, in contrast to the SSH model [11], which makes the transition to be the second order.

The phonon part H_{ph} of (1) is given as

$$H_{ph} \equiv \sum_{\ell}\frac{S_1}{2}(q_{\ell} - q_{\ell+1})^2 + \sum_{\ell}\frac{S_2}{4}(q_{\ell} - q_{\ell+1})^4 \tag{5}$$

wherein a fourth-order potential with a coefficient S_2 is introduced, as well as the ordinary second-order S_1, while the kinetic energy of phonons are neglected because of the adiabatic approximation.

As for the inter-chain interaction H_{inter}, we neglect it in the study for the ground state properties. This inter-chain interaction is tacitly assumed to be so small as to give almost no contribution provided that the ground state is uniform for all the chains in the crystal, whether it is the dimerized I-phase or the monomeric neutral one. Only if a large and macroscopic domain appears in the I-phase, is this inter-chain interaction assumed to bring an appreciable energy increase. We give its practical form later in detail.

Using this model Hamiltonian, let us now set up our simplistic picture for both the I- and N-phases. The N-phase is such that the HOMO of the TTF is filled with two electrons of opposite spins ($\uparrow$ and $\downarrow$), while the LUMO of the CA is vacant, as schematically shown in figure 4(a). Thus, the two constituent molecules are literally neutral, while the electronic state realized in this system is just equal to the charge density wave (CDW) state of the double

period. On the other hand, the I-phase is such that the HOMO and the LUMO are alternately occupied by the electrons of ↑ and ↓ spins as shown in figure 4(b). Within this picture, this state is just equal to the spin density wave (SDW) state of the double period. However, as shown in figure 4(b), this I-phase also has the dimerization between neighbouring TTF and CA molecules.

Here we should note why (4) is nonlinear and (5) is anharmonic. If we retain only the linear term in (4), the energy gain due to the dimerization in the I-phase cancels between left and right of each molecule, since our system is not a single ionic pair but a 1D chain crystal. For this reason, the nonlinear term is introduced in (4). Accordingly, the quartic anharmonicity is also introduced in (5). It comes from the inter-molecular repulsion, and prevents unphysically large dimerizations.

In our theory, we have eight parameters: T_i, Δ, U, V_0, β_1, β_2, S_1 and S_2. The values of these parameters are determined so that they, as a set, reproduce the main experimental and theoretical results already existing prior to our theory. For T_i, we use the *ab initio* calculation by Katan [14]. On the other hand, from spectroscopic studies in the visible and infrared regions, the total charge induced at the CA site of the I-phase is determined to be $\rho_I = 0.8$ [15]. By the same experiment, the total charge induced at the CA site of the N-phase is determined as $\rho_N = 0.3$. Unlike the simplistic picture shown in figure 4, these induced charges ρ_I and ρ_N are not natural numbers such as 1 or 0, but are fractional, because the valence electrons are quantum mechanically itinerant, as denoted by the non-zero value of T_i. In addition to these, there are the following five well known experimental results. By the x-ray structure analysis, the dimeric displacement of each molecule in the ionic ground state is determined to be 2.5% of the original intermolecular distance [8]. Moreover, in the light absorption spectrum of the I-phase, two CT absorption peaks appear at 0.6 eV and 1.0 eV with an intensity ratio 1: 0.5, while, in the N-phase, only a single CT peak appears at 0.6 eV [15]. Using these data, we can determine our eight parameters without serious ambiguity as $T_i = 0.17$ eV, $\Delta = 2.716$ eV, $U = 1.528$ eV, $V_0 = 0.604$ eV, $\beta_1 = 1.0$ eV, $\beta_2 = 8.54$ eV, $S_1 = 4.86$ eV and $S_2 = 3.4 \times 10^3$ eV.

5.2. Ground state properties

Let us now consider the properties of the ground state given by this Hamiltonian H, using the unrestricted Hartree–Fock approximation. Within this approximation, we can reduce the two-body terms of H_{el} into one-body terms as

$$U n_{\ell,\alpha} n_{\ell,\beta} \to U(n_{\ell,\alpha}\langle n_{\ell,\beta}\rangle + \langle n_{\ell,\alpha}\rangle n_{\ell,\beta} - \langle n_{\ell,\alpha}\rangle\langle n_{\ell,\beta}\rangle) \tag{6}$$

$$V_\ell n_\ell n_{\ell+1} \to V_\ell \Big\{ (n_\ell\langle n_{\ell+1}\rangle + \langle n_\ell\rangle n_{\ell+1} - \langle n_\ell\rangle\langle n_{\ell+1}\rangle) - \sum_\sigma (\langle m^+_{\ell,\sigma}\rangle m_{\ell,\sigma} + m^+_{\ell,\sigma}\langle m_{\ell,\sigma}\rangle - \langle m^+_{\ell,\sigma}\rangle\langle m_{\ell,\sigma}\rangle) \Big\} \tag{7}$$

$$m_{\ell,\sigma} \equiv C^+_{\ell,\sigma} C_{\ell+1,\sigma} \tag{8}$$

where $\langle\cdots\rangle$ denotes the expectation value of operator .... This is unknown at the present stage, but will be determined later self-consistently. Since our system is the half-filled system wherein the total number of the lattice sites (N_t) is equal to the total number of electrons as

$$\frac{N_t}{2} = \sum_\ell n_{\ell,\alpha} = \sum_\ell n_{\ell,\beta} \tag{9}$$

we assume for $\langle n_{\ell,\sigma}\rangle$, $\langle m_{\ell,\sigma}\rangle$ and q_ℓ the following forms with the double period:

$$\langle n_{\ell,\sigma}\rangle = \tfrac{1}{2} + (-1)^\ell \delta n_\sigma \qquad \langle m_{\ell,\sigma}\rangle = \overline{m}_\sigma + (-1)^\ell \delta m_\sigma \qquad q_\ell = (-1)^\ell q_0 \tag{10}$$

where δn_σ, $\overline{m}_\sigma$, δm_σ and q_0 are to be determined within the Hartree–Fock and adiabatic approximations.

The Hartree–Fock-type self-consistent equation for these δn_σ, $\overline{m}_\sigma$ and δm_σ gives two solutions for given q_0, corresponding to the I-phase with $\delta n_\alpha \approx -\delta n_\beta$ (SDW) and to the N-phase with $\delta n_\alpha \approx \delta n_\beta$ (CDW). In figure 5, we have shown the total energy E_g thus theoretically calculated as a function of q_0, and these I- and N-phases are shown to be pseudo-degenerate with each other. The energy minimum of the I-phase is 0.002 eV lower that of the N-phase, and they are separated by an adiabatic energy barrier of about 0.0045 eV. Thus the I-phase is the true ground state, while the N-phase is the false one, and both phases are locally stable. Furthermore, the I-phase is theoretically shown to be dimerized about 2.9% of the lattice constant, while the N-phase is not dimerized ($q_0 = 0$). Although we have been concerned only with the adiabatic energy at absolute zero temperature, the presence of the aforementioned adiabatic energy barrier means that the ordinary thermal phase transition between N-phase and I-phase is of first order.

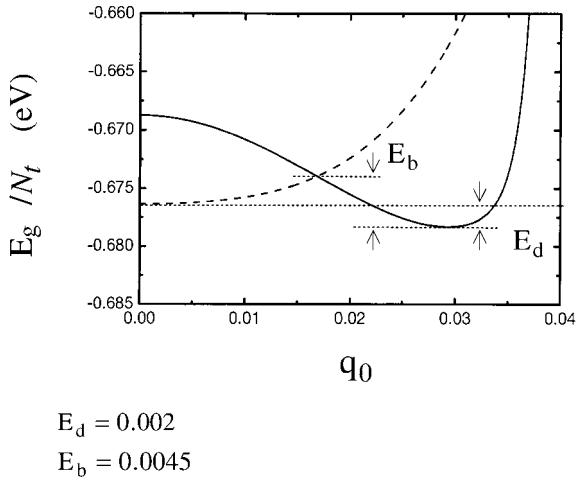

Figure 5. Total energy per site for neutral (- - - -) and ionic (——) phases as functions of q_0 [7].

In figure 6(a), we have illustrated the charge and the spin density distributions calculated for the I-phase. This phase is characterized by the strong SDW order ($\delta n_\alpha \approx -\delta n_\beta \approx 0.4$) mixed with a weak CDW-type order. The calculated induce charge ρ_I is 0.95, being quite large but still fractional. Figure 6(b) demonstrates the N-phase, and there is only the CDW-type order ($\delta n_\alpha \approx \delta n_\beta \approx 0.4$). The calculated induced charge ρ_N of this phase is 0.2, being comparatively small, but still significant due to the finiteness of T_i.

5.3. Energy band structure and lowest excited state

Figure 7(a) presents four one-electron energy bands of the I-phase, obtained as functions of a wavevector, by using this unrestricted Hartree–Fock approximation. It has an antiferromagnetic broken symmetry in the spin space. There are two bands for each up- and down-spin electron as distinguished by the arrows in figure 7(a). In the ground state, the two lower bands are occupied, while others are vacant. The lowest band, being occupied by up-spin electrons, is mainly composed of the LUMO of TTF, while the second lowest band, being occupied by down-spin electrons, are mainly composed of the HOMO of CA. In this

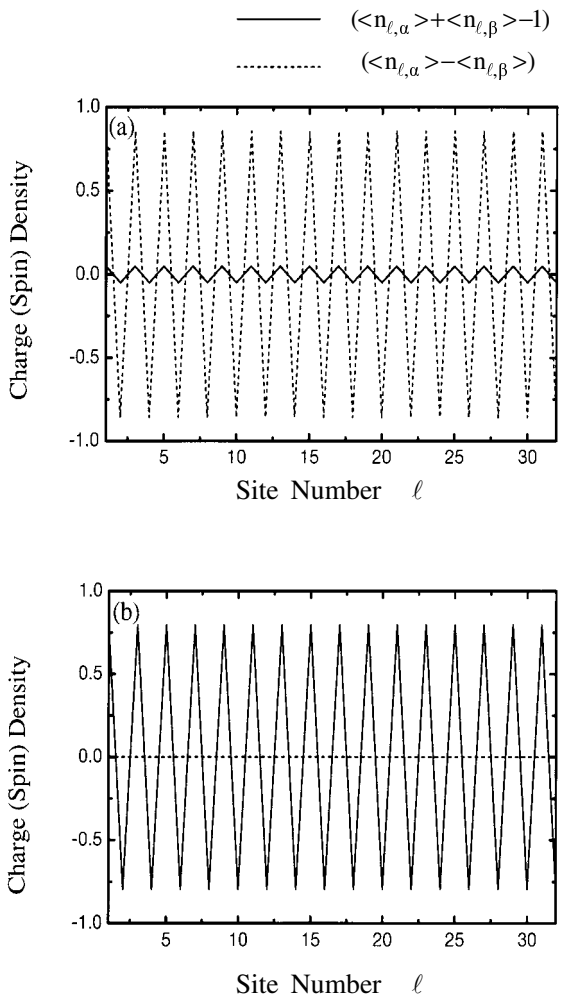

Figure 6. Charge and spin densities of (a) ionic and (b) neutral phases as functions of ℓ [7].

system, the elementary optical excitation is such that a down-spin electron goes from the second lowest band to the third one, as shown by a dashed arrow in figure 7(a). This third band is mainly composed of the HOMO, which is already occupied by an up-spin electron, and hence the excitation energy partly due to U in (2).

If we change our picture from the wavevector space to the real space, this excitation results in a doubly occupied HOMO and a vacant LUMO, while all other sites still keep the original single occupancy. The electron and the hole thus created by light attract each other through $-V_\ell$, and make the aforementioned bound state called the CT exciton, as schematically shown in figure 7(b), which is the same as the one already shown in figure 2(b). This is the lowest Franck–Condon-type excited state, calculated by our theory based on the unrestricted Hartree–Fock approximation, reinforced by including the electron–hole attraction at the final state of the optical transition [7]. Using this reinforced theory, we have also calculated the spectral shape of the CT excitation including classical lattice fluctuations [7]. The resultant spectral shape has two peaks at 0.6 and 1.0 eV in the case of the I-phase, while, in the case of

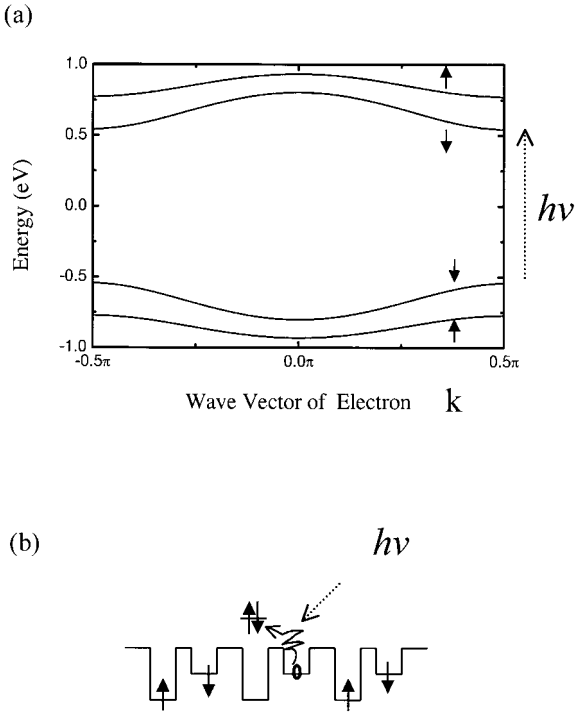

Figure 7. (a) The energy bands in the ionic phase. The lower two bands are occupied by up and down spin electrons as denoted by corresponding arrows. The dashed line denotes the lowest excitation in the band picture. (b) Schematic illustration of the charge transfer excitation in real space [7].

N-phase, it has a single peak at 0.6 eV. Thus, our theory can successfully reproduce the known experimental results.

5.4. Relaxation path

Let us now proceed to the lattice relaxation path of optical excitations. The visible photon has a long wavelength of about 1000 times the lattice constant, and each photon can make a single CT exciton per this length. Among many excitons thus created in the whole ionic crystal, we will focus only on a single CT exciton and will clarify its lattice relaxation path. This path starts from the Franck–Condon state, and terminates up to the macroscopic N-domain formation. In order to describe this path theoretically, we introduce the following lattice distortion pattern q_ℓ:

$$q_\ell = (-1)^\ell q_0 \left\{ 1 + \Delta q \left[\tanh\left(\theta \left(|\ell| - \frac{\ell_0}{2} \right) \right) - 1 \right] \right\}. \tag{11}$$

Here $(-1)^\ell q_0$ denotes the dimeric distortion of the ionic ground state from which we start. The second term in the curly brackets $\{\cdots\}$ denotes a local lattice displacement induced by a new excited domain. Δq is its amplitude, θ corresponds to the width of the domain boundary, and ℓ_0 is the domain size. Typical domain structures given by these parameters are demonstrated in figure 8. When $\Delta q < 0.5$, the lattice inside of the domain has a reduced dimerization, but is still in the same phase as the original lattice outside of the domain, and hence it corresponds

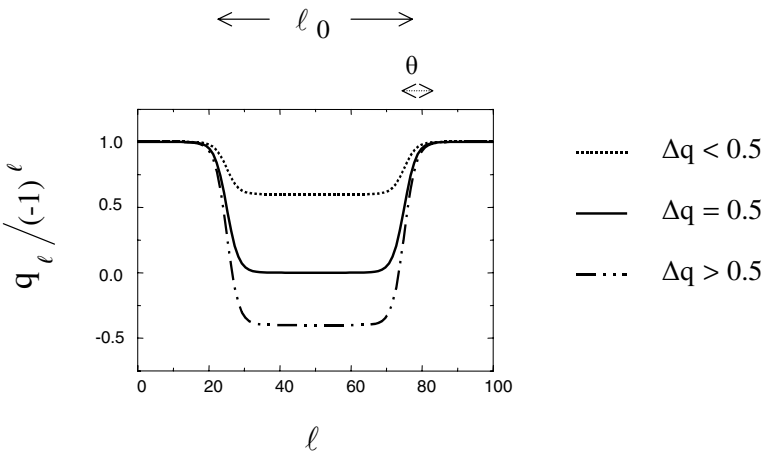

Figure 8. The lattice distortion pattern to describe the relaxation as a function of ℓ. ℓ_0 is the domain size. θ is the width of the domain boundary.

to a new I-domain. In the case of the second situation $\Delta q = 0.5$, it is obvious that the inside lattice has no dimerization at all. Therefore, it corresponds to a N-domain.

Let us return to the problem of H_{inter}. The distance between the TTF and the CA molecules within a chain is about 3 Å, while the inter-chain distance is about 10 Å, and hence, as mentioned before, we have neglected this interaction, assuming that it will give no serious effect. Even for the excited domain, this situation will be same, if the new displacement $(q_\ell - (-1)^\ell q_0)$ associated with this new domain is small as compared with the original displacement in the ground state, $|q_\ell - (-1)^\ell q_0| \leqslant q_0$. On the other hand, when the new displacement becomes very large, $|q_\ell - (-1)^\ell q_0| \gg q_0$, various inter-molecular repulsions will also act, and will give a nonlinear increase of the lattice potential, just as shown in equation (5) and figure 5. Moreover, this effect will become appreciable only when the new domain expands to a macroscopic size in a single chain. To take this nonlinear inter-chain interaction into account effectively, we use the following form:

$$H_{inter} = \sum_\ell \left\{ K_1(q_\ell - (-1)^\ell q_0)^2 + K_2(q_\ell - (-1)^\ell q_0)^4 + K_3(q_\ell - (-1)^\ell q_0)^6 \right\} \tag{12}$$

where q_ℓ denotes the lattice distortion of a central chain on which we focus, while $(-1)^\ell q_0$ is the representative of the displacements of environmental chains, and $K_i (i = 1, 2, 3)$ denotes the $2i$th expanding coefficient with respect to the new distortion. These environmental chains are assumed to be frozen in the ionic ground state, being never excited whatever occurs in the central chain. For practical calculations, we take the following values: $K_1 = 0.6949$ eV, $K_2 = -1.415 \times 10^3$ eV and $K_3 = 9.699 \times 10^5$ eV. These values are so chosen that the interchain interaction becomes appreciable only when $|q_\ell - (-1)^\ell q_0| \geqslant 2q_0$ and $\ell_0 \geqslant 10^2$.

Figure 9 demonstrates the adiabatic energy surface of the ground state E_g and that of the first excited state E_{x1} thus obtained, as a function of Δq and ℓ_0. θ is determined to minimize E_{x1}, since we are going to clarify the relaxation path of the excited state. All the energies are referenced from the energy of the ionic true ground states ($\Delta q = 0$, $\ell_0 = 0$) shown in figure 5. In figure 9(a), the region with $\Delta q < 0.5$ is still the I-phase, which has the SDW-type order already shown in figure 6(a). In the plateau region ($\Delta q \cong 0.5$ and $\ell_0 \geqslant 40$) of figure 9(a), the N-domain appears, and it has the CDW-type order just as in figure 6(b). We have various shallow local minima in this plateau region, an example of which is shown in the enlarged

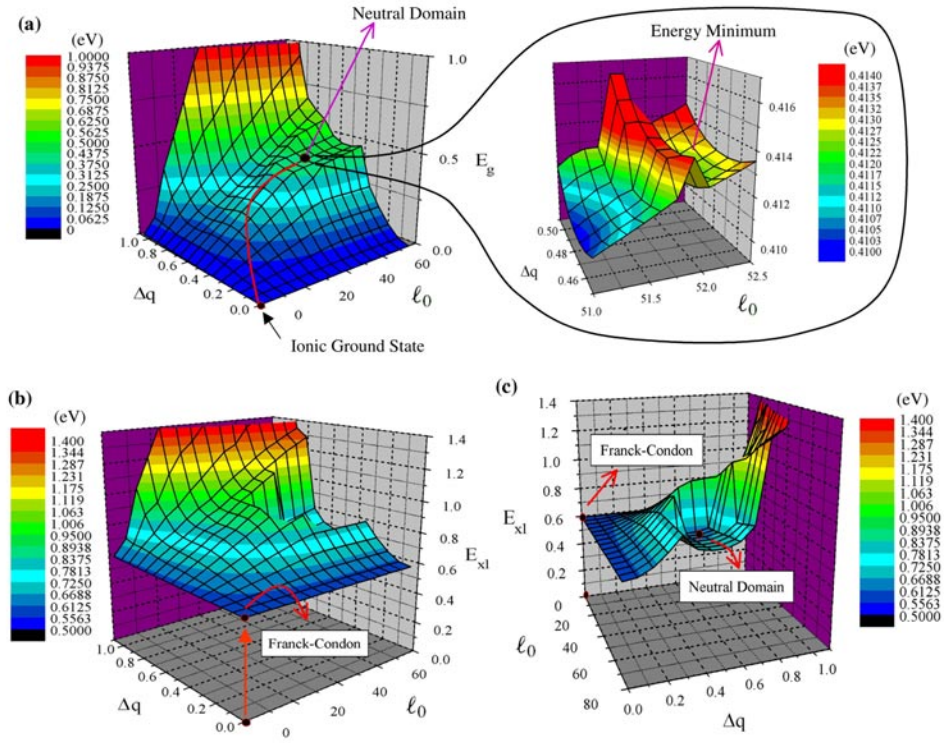

Figure 9. The calculated adiabatic energy surfaces in two-dimensional space spanned by Δq and ℓ_0. (a) The ground state E_g. The grey line denotes the steepest ascending line from the ionic true ground state to the neutral domain. The enlarged inset denotes one of the local energy minima. (b) Front view of the lowest excited state E_{x1}. (c) Back view of the lowest excited state E_{x1}. All the energies are referenced from the ionic true ground state [7].

inset to figure 9(a). The presence of these local minima is mainly due to the discreteness of the lattice, and makes the N-domain stable and long-lived. As Δq and ℓ_0 increase further ($\Delta q \geqslant 0.5$, $\ell_0 \geqslant 50$) from this plateau region, E_g also increases further. This increase is mainly due to H_{inter} given by (12), and partly due to the intrinsic energy difference between the I-phase and the N-one shown in figure 5.

Figures 9(b) and 9(c) show front and back views of the adiabatic energy surface of the lowest excited state E_{x1}. At the origin ($\Delta q = 0$, $\ell_0 = 0$), or at the Franck–Condon state, a local minimum appears, and it is due to the CT exciton. There is another local minimum at around $\Delta q = 0.5$ and $\ell_0 = 45$. It corresponds to an excited state of the N-domain, which has the same CDW-type order as that of the ground state, except for the domain boundary shown in figure 2(c) by the two dashed lines. As Δq and ℓ_0 increase further ($\Delta q \geqslant 0.5$, $\ell_0 \geqslant 50$), E_{x1} also increases further. This increase is again mainly due to H_{inter}, and partly due to the intrinsic energy difference between the I-phase and the N-one. Thus, H_{inter} is essential to make the N-domain locally stable.

In figure 10, we have shown both E_g and E_{x1} as a function of ℓ_0, along the steepest ascending line from the true ionic ground state to the N-domain. This line, denoted by grey in figure 9(a), is determined to be always orthogonal to the equi-potential line. In the adiabatic energy curve of E_{x1}, we can see the two local minima mentioned before. The first one at $\ell_0 = 0$ corresponds to the CT exciton. While the second one at $\ell_0 = 45$ corresponds to the N-domain,

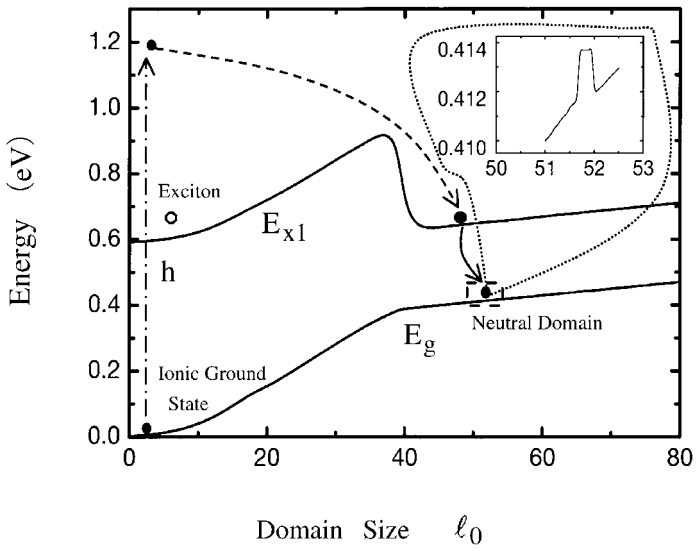

Figure 10. Adiabatic energies of the ground state E_g and the lowest excited state E_{x1} along the steepest ascending line. The dashed curve denotes the expected relaxation path to generate the neutral domain. The enlarged inset denotes one of the local minima in the ground state [7].

which is a little above the CT exciton. These two minima are clearly separated by a high adiabatic potential barrier with each other. As shown in figure 2(c) by the two dashed lines, we have two boundaries between the I-phase and the N-phase. The energy increase to create these two boundaries makes a small size N-domain ($\ell_0 < 40$) too unstable in the excited state. It can be stable only when its size exceeds a critical value ($\ell_0 \approx 40$), just like the formation of a gaseous bubble in an overheated liquid. We should also note that it is the characteristic only of the excited state E_{x1}. In the ground-state energy curve E_g shown in figure 10, we have no such high barrier, but only low barriers as shown in the enlarged inset.

Thus, we can conclude that the single CT exciton alone can never result in the N-domain formation directly. Only when our system is excited by a large excess electronic or vibrational (phonon) energies over the single exciton state can it overcome this high barrier and result in N-domain formation, as shown in figure 10. In other words, only when we have such a large excess energy at the very beginning of the relaxation, can this excess energy be converted into the exciton proliferation, and induce various other nonlinear processes during the relaxation.

Finally, it should be noted that the process described above is only the early stage or the nucleation process of the macroscopic photoinduced phase transition. The neutral domain thus created will stay in the shallow minimum for a longer time than the one oscillation period of phonon. Hence, during this stay, it can move diffusively within a chain, and can aggregate with other N-domains created by other photons, and result in a global phase transition.

5.5. High-energy optical excited states in SDW state

As mentioned above, the high-energy optically excited states are responsible for the photoinduced phase transition, rather than the single CT exciton. Hence, we have to clarify the nature of these highly excited states of the SDW state. In the Franck–Condon state, as mentioned before, quantum and dynamical natures of the electron–phonon interaction do not work, since the lattice is fixed at the ground-state configuration. As is well known, the

electron–phonon interaction is a retarded one, which can start working quantum mechanically about 10^{-12} s after the optical excitation. The inter-electron Coulomb interaction, being the instantaneous force, will dominate the nature of highly excited states, since the starting ground state is the SDW state. In order to clarify this effect, however, the unrestricted Hartree–Fock approximation is too crude, and we have to take into account effects of quantum fluctuations of itinerant electrons due to the Coulomb interaction. For this reason, we clarify higher optical excited states of the half-filled SDW state, using a simplified one-dimensional extended Hubbard Hamiltonian

$$H_{ex} = -T_i \sum_{\ell,\sigma} [(C^{+}_{\ell,\sigma} C_{\ell+1,\sigma}) + \text{HC}] + U \sum_{\ell} n_{\ell,\alpha} n_{\ell,\beta} + V_0 \sum_{\ell} n_{\ell} n_{\ell+1}. \tag{13}$$

When $U > 2V_0$, this Hamiltonian gives the SDW state with the antiferromagnetic order, as figure 4(b), although we have neither Δ nor the dimeric electron–phonon interaction. When $U < 2V_0$, we have the CDW state just as figure 4(a). When U exceeds $2V_0$ only a little, we get a situation similar to figure 5, that this SDW state is just below the CDW one. Thus, as far as the Franck–Condon states are concerned, we can well reproduce the situation realized in the TTF-CA crystal, using this simple model. The benefit of this simple model is that we can calculate higher excited states, using the non-Grassmann path-integral theory [16, 17], which takes the Coulombic inter-electron quantum correlations straightforwardly. By this theory, various optical spectra have been calculated under the bistable condition $(U - 2V_0) \ll U$ [16, 17]. From these results, we can conclude that high-energy optical excited states with energies a few times greater than the CT exciton are the random excitations of several CT excitons coupled with many magnons or spin-excitations. As is well known, in the SDW state, we have the Goldstone mode called magnon, whose energy is gapless and has a linear dispersion. When the SDW state has a small dimerization, a small energy gap opens in this dispersion. However, the above characteristic of high-energy excited states is not affected.

One might consider the possibility that a macroscopic CDW domain (N-domain) could be directly excited just after the Franck–Condon transition from the SDW ground state, by using only a few photons. However, this is impossible since these two states are macroscopically orthogonal with each other. It is theoretically obvious that a dipole operator of a photon can change the state of only one electron, before and after the transition. An electron and a hole thus created by this dipole transition can also change the states of many other surrounding electrons through the Coulomb interaction. However, this is nothing other than random scattering, being far from making a well defined macroscopic spatial order at once. The macroscopic spatial order can be established only after this highly excited state is cooled to some local minimum, dissipating its excess energy one by one into the phonon system, which acts as a heart reservoir, as shown in figure 10. This is the essence of lattice relaxation and the macroscopic order formation.

6. Early-time nonlinear non-equilibrium quantum dynamics and initial condition sensitivity

So far, we have been concerned only with the adiabatic natures of the TTF-CA. We now proceed to the early-time nonlinear non-equilibrium quantum dynamics of the PSPT. To theoretically describe this dynamics, however, the practical situation realized by (1) is too complicated. Hence, we have to simplify our problem, extracting only its essential points from the viewpoint of the PSPT.

(1) When the exciting photon is resonated to the CT exciton ($\sim$0.6 eV), these excitons are created homogeneously in the 1D crystal, and hence the mean inter-exciton distance

becomes rather long as compared with the lattice constant. Just after the intra-molecular excitation (∼2.2 eV), an electron–hole pair is created in a same molecule, with energy a few times greater than the CT exciton. This high-energy pair is electronically unstable even at the Franck–Condon state, and will immediately decompose into several CT excitons, through inter-molecular Auger decays or other Coulombic many-body scatterings. These several CT excitons are expected to be very close to each other around the original molecule. Therefore, the difference in the initial condition between the CT excitation and the intra-molecular one is reduced only to the difference of the initial distance between the adjacent photogenerated CT excitons. We also have many other excitations in between (0.6–2.2 eV), and the corresponding spatial arrangements of the CT excitons will be different from each other, even if the total absorbed photonic energies are the same. To describe this difference, we have schematically shown, in figure 11, three typical cases of such spatial arrangements: (a) sparse, (b) close and (c) moderately distant excitations. Using these three typical arrangements of excitons, we will clarify the initial condition sensitivity.

(2) There must be a hidden but intrinsic multi-stability. A false ground state has to be just above the true one, and the energy difference between them per unit volume should be larger than the thermal energy, but much smaller than the visible photon energy, as schematically shown in figures 1, 5, 10 and 12.

(3) There must be a nonlinear mechanism through which the excitons can proliferate. This mechanism should be efficient enough to overcome various radiative and non-radiative decay channels of the CT excitons. These decay channels will act in every intermediate stage of the relaxation to hinder the proliferation, as schematically shown in figure 12.

(4) At the final state of the Franck–Condon transition, a large excess energy should be given to the excitons, as schematically shown in figures 10 and 12. By using these excess energies, the initially created excitons can proliferate, under the energy conservation law.

(5) The resultant domain should be a local minimum in the adiabatic potential surface of the ground state, so that this domain can have a sufficiently long lifetime worthy to be called PSPT. Thus, the initially created excitons have to go through various intersections of the potential surfaces diabatically, so that they can finally reach the local energy minimum, not in the excited state potential surface, but in the ground-state one, as shown schematically in figure 10 and 12.

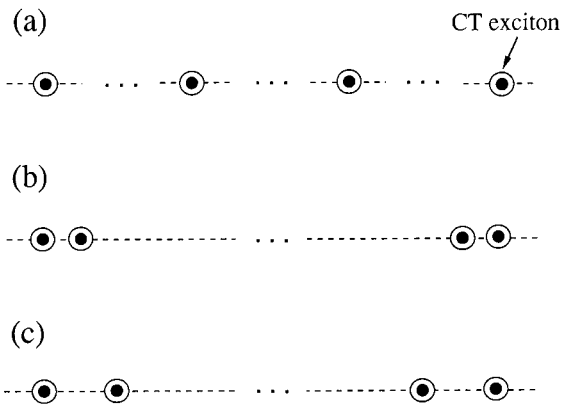

Figure 11. Schematic illustrates of CT exciton excitations with various distances. (a) Sparse, (b) close and (c) moderately distant excitations.

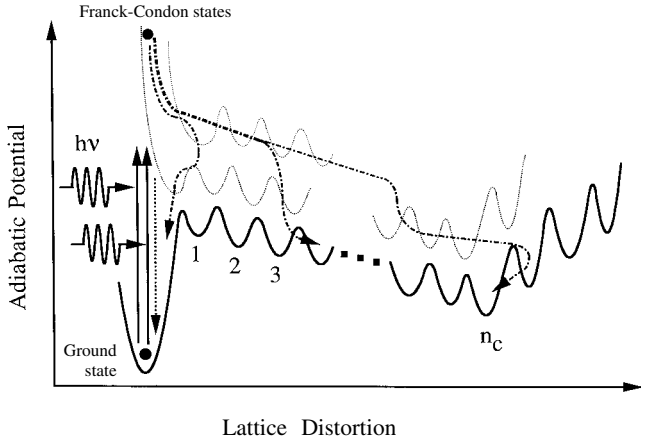

Figure 12. Schematic illustration of the dynamics of exciton relaxation and the domain formation.

6.1. Model Hamiltonian for quantum dynamics

In order to describe the above points from a unified theoretical point of view, we will use a more simplified model than (1), and will clarify the early-time quantum dynamics of the PSPT. For this reason, we take the following many-exciton system coupling strongly with Einstein phonons in a quasi-1D crystal [18, 19]. Its Hamiltonian (H_{me}) is given as

$$H_{me} = E_e \sum_\ell B_\ell^+ B_\ell - T_e \sum_\ell [B_\ell^+ B_{\ell+1} + \text{HC}] + \omega \sum_\ell b_\ell^+ b_\ell - \omega S^{1/2} \sum_\ell B_\ell^+ B_\ell (b_\ell^+ + b_\ell)$$
$$- V_e \sum_\ell B_\ell^+ B_\ell B_{\ell+1}^+ B_{\ell+1} + \sum_{\ell,\ell'(\neq\ell)} G(|\ell - \ell'|) B_\ell^+ B_\ell (B_{\ell'}^+ + B_{\ell'}) + H_{ie} \qquad (14)$$

where B_ℓ^+ is a creation operator of an exciton (a boson) at a site ℓ with an energy E_e, and T_e is its inter-site transfer energy. b_ℓ^+ is the creation operator of the Einstein phonon at site ℓ with a frequency ω, and S is the exciton–phonon coupling constant. V_e denotes a phenomenological inter-exciton attraction. In the present theory, we will not specify its microscopic origin. It can be an effective attraction due to the van der Waals force, other Coulombic interactions, or some inter-site exciton–phonon couplings. The occupancy of a single site by more than one exciton is excluded from the beginning. $G(\ell - \ell')$ in the sixth term represents the third-order anharmonic inter-exciton coupling. Through this anharmonicity, an exciton at site ℓ' is created or annihilated by another exciton at site ℓ. Such a nonlinearity results from the long-range Coulomb interaction between electrons and holes constituting excitons. The Coulomb interaction is originally quartic with respect to these Fermion operators, being quite nonlinear from the beginning. Hence, to take into account this nonlinearity or anharmonicity is quite natural. However, through this nonlinearity the excitons can proliferate, as shown later in detail. Furthermore, since this Coulombic nonlinearity is an instantaneous force with no retardation effect, it can cause the proliferation readily.

The last term H_{ie} denotes the interchain interaction:

$$H_{ie} = \sum_n h(n) \sum_i |n, i\rangle\langle n, i| \qquad (15)$$

where n denotes the total number of the excitons, and i specifies each quantum state $|n, i\rangle$ within n exciton states. Thus, $\sum_i |n, i\rangle\langle n, i|$ is a projection operator into the n-exciton state. $h(n)$ denotes an effective potential given from the other chains to this n-exciton system, when

it is created in the central chain on which we focus. This potential $h(n)$ is assumed to depend only on the total number n, irrespective of various spatial arrangements of n excitons. The functional form of $h(n)$ is also assumed to be quite nonlinear in the sense that it is almost zero when n is smaller than its critical value n_c, while it becomes nonlinearly appreciable when n exceeds n_c. The role of this interaction is almost same as that of (12), and it makes the domain with n_c excitons locally stable, as schematically shown in figure 12.

It should be noted that the present exciton–phonon system is our relevant system, and is also assumed to couple linearly with the photon field and acoustic phonon modes, which act as a heat reservoir during the relaxation, although they are not written here explicitly.

6.2. Relaxation and occurrence or non-occurrence of the PSPT

Using figure 12, let us now schematically explain the characteristics of the relaxation processes, which lead to the occurrence or non-occurrence of the PSPT. The solid curve and thin dotted curves denote adiabatic potential surfaces of the ground and excited states. The global minimum of the lowest curve denotes the ground state. The other local minima 1, 2, ... of this curve denote the lowest energy states with 1, 2, ... excitons, respectively. The local minimum n_c has the lowest energy among these local minima 1, 2, ... The upward solid arrows denote the initial photoexcitations. The dash-dotted arrows denote the main relaxation paths. The downward dotted arrow denotes radiative decay of excitons. These non-radiative and radiative decays are brought about through the interaction between our relevant system and the acoustic phonon or photon fields mentioned before. We also have assumed a multi-stable situation where the lowest energy of $(n+1)$-exciton state is energetically close to that of n-exciton state. This condition is realized when $(E_e - S)$ and V_e are well balanced in (15), as $(E_e - S) \approx V_e$.

In figure 12 the excitons are created from the ground state by photoabsorption (the leftmost upward solid arrows). Then, the exciton relaxes along the following two paths. One path is the vibrational (or lattice) relaxation, where the system changes along an adiabatic potential curve of the excited state (the dash-dotted curves in figure 12). The photoexcited state along this path has large excess electronic and vibronic (phonon) energies. The other path is the direct radiative decay (the downward thick dotted arrow in figure 12). Here, the former path is the main one because vibrational relaxation is faster than radiative decay. As seen from the figure, many adiabatic potential surfaces come close to each other at many points. Around such points, the diabatic transition occurs. If the relaxation proceeds toward the right through such processes, the proliferation becomes successful.

As mentioned in section 4, various relaxations can start from almost the same Franck–Condon states, as long as the initially absorbed total photonic energies are same. However, these starting points are slightly different from each other, depending on the photoexcitation, because their electronic structures are different. During the relaxation, the initial small difference increases. Some quickly return to the ground state non-radiatively, while others proceed toward the right in figure 12 and stay in multi-exciton state for a long time. This is the initial condition sensitivity mentioned before. Furthermore, among the latter cases, some quickly reach the lowest energy state with n_c excitons, while others, because of the tunnelling, rather slowly reach the n_c exciton state, although they relax quickly to the lowest potential curve.

Here we emphasize about the prolongation of the lifetime of these various transient states, which appear during the relaxation. As mentioned above, the PSPT is a transient phenomenon, and the system always returns to the ground state. However, the state generated by the PSPT can become relatively stable, and take a long time to return to the ground state. This is because the overlap integral between the multi-exciton state and the ground state becomes smaller and smaller, as the proliferation proceeds from left to right in figure 12. Hence the transition

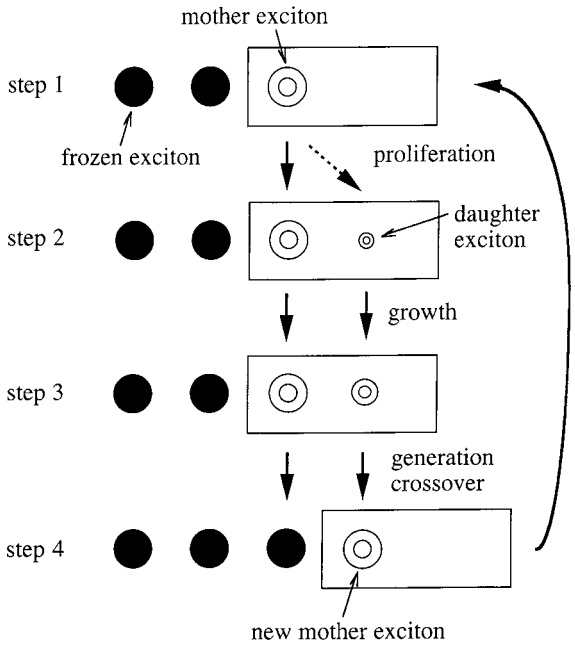

Figure 13. Schematic illustration of the iterative equation, and the generation crossover.

between them becomes very difficult, even if the photon and the acoustic phonon spontaneously try to induce it, through their quantum fluctuations. Thus, the more the decay time elongates, the more the resultant domain becomes large and stable.

6.3. Derivation of iterative equation for exciton proliferation

In order to investigate the time evolution of the aforementioned exciton–phonon system, we are now at the stage to derive the master equation under the Markov approximation for the photon field and the reservoir. However, there is a serious numerical difficulty in the direct calculation of this time evolution in large systems, because the quantum mechanical treatment of Einstain phonons leads to too large dimensional calculations. Therefore, in order to overcome this numerical difficulty, we derive the iterative equation for the exciton proliferation. The basic idea is schematically shown in figure 13.

We focus only on the front of the expanding photoinduced domain, and the contributions from the other excitons, not at this front, are approximated by a mean field. As proliferation proceeds, the position of this front also moves. At step 1 in figure 13, the front of the domain is assumed to be inside the box. This box is our relevant system, within which we calculate excitons, Einstein phonons and their interactions, fully quantum mechanically. We take the size of the box as four lattice sites around the front. Inside of this box, we prepare an exciton with an excess energy, represented by a double circle. We call this the 'mother exciton'. We also prepare several excitons outside of our relevant system (the box), and they are represented by black circles.

They are localized at each lattice site, and their energies are fixed to the lowest vibronic ones. We call them 'frozen excitons'. The mother exciton can proliferate through $G(\ell - \ell')$ in (15) by using her excess energy, and can make her 'daughter exciton' (step 2 in figure 13).

Through $G(\ell - \ell')$ in (15), the frozen excitons can also help this proliferation as an external mean field, given as

$$\sum_{\ell,\ell'(\neq\ell)} G(|\ell - \ell'|)\langle B_\ell^+ B_\ell\rangle (B_{\ell'}^+ + B_{\ell'})$$

where $\langle B_\ell^+ B_\ell\rangle$ denotes the frozen exciton density at that site.

As time goes by, this daughter exciton grows up, and the total number of excitons increases (step 3 in figure 13). When the total number of excitons in the front increases by one, we consider that the daughter has grown up to be an adult, and approximate that the following generation crossover occurs (step 4 in figure 13). The mother exciton is replaced by a frozen one, and the daughter exciton is taken as a new mother. Here, as seen from (15), it should be noted that excitons (except frozen ones) can move between lattice sites in the box. Thus, the exciton density has a non-integer value at each lattice site. Therefore, in the aforementioned crossover, we regard the excitons whose densities are the largest and the second largest in the box as the mother exciton and the daughter one, respectively. Furthermore, we assume that the new mother inherits the excess energy, after this crossover. We determine this excess energy of the new mother so that the total energy in the system is conserved before and after this crossover. It becomes smaller and smaller than the starting one, because of the dissipation or relaxation.

By this crossover, the front moves, and accordingly the box moves. In fact, in the case of figure 13, the front moves one lattice site towards the right. Then, we focus again only on this new front, and iterate the aforementioned procedure, until the excess energy is exhausted through the interaction between our relevant system and the aforementioned heat reservoir. During this procedure, the size of the box around the front is kept unchanged. Therefore, without enlarging our computer memory, we can numerically calculate the time evolution dynamics of a large number of excitons in a large system.

This iterative procedure is justified when T_e is small as compared with $S\omega$ in (15).

6.4. Numerical results

Let us now specify the values of the parameters in (15). Our purpose here is not a comprehensive study for (15), but to study one of typical situations realized by a set of parameter values, which is in compliance with the aforementioned five points, and makes the PSPT successful. As one such example, the following values are taken: $\omega = 0.1$ eV ($\hbar = 1$), $E_e/\omega = 9.5$, $T_e/\omega = 1.0$, $S = 8$, $V_e/\omega = 1.7$, $G(1)/\omega = 0.2$, $G(2)/\omega = 0.1$, $G(3)/\omega = 0.067$, $G(4)/\omega = 0.05$, $G(5)/\omega = 0.04$ and zero for other G. n_c is taken to be 10. The radiative damping rate of the exciton is assumed to be 10^{-9} s at the Franck–Condon state, and afterward decreases in proportion to the third power of the transition energy, while the damping of the Einstein phonon due to its coupling with the acoustic phonon reservoir is assumed to be 20% of the phonon energy ω. The large S corresponds to the large excess energy at the Franck–Condon state, while finite ω/T_e makes diabatic transitions possible.

We start from the initial condition that there are two localized excitons, just as shown in figure 11. One of them is an exciton created by the Franck–Condon excitation from the ground state. This is a mother exciton. The other exciton is taken as a frozen one, for the reason mentioned before. In the following, the distance between these two excitons at the initial state is represented by d_0. Results are shown in figure 14, and the time evolution dynamics become different according to this d_0. The net exciton proliferation occurs only when $d_0 = 2$, 3 and 4. When $d_0 = 1$ and ∞, the number of excitons increases a little from 2 only at early time. However, the net proliferation does not finally occur. Therefore, the initial distance between excitons should be moderate in order to get net proliferation. In the too-far distant case ($d_0 = \infty$), the nonlinearity among excitons does not work, and leads to no net proliferation.

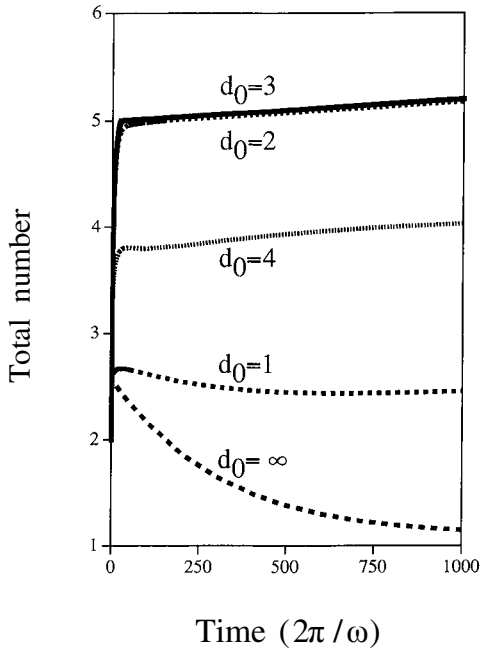

Figure 14. The total number of exciton as functions of time. d_0 is the distance between initial two excitons [18, 19].

On the other hand, in the too-close excitation case ($d_0 = 1$), too-strong nonlinearity works, and leads to exciton annihilation rather than its proliferation. Therefore, the critical nonlinearity is necessary to realize net proliferation. Here, the case with $d_0 = \infty$ corresponds to the CT excitation below the threshold mentioned in section 3. In the intra-molecular excitation case, d_0 takes various values within the force range of the aforementioned intermolecular Auger decay. Among them, only the successful cases can finally survive ($d_0 = 2$, 3 and 4). Furthermore, even when the net proliferation occurs, the time evolution behaviour of each proliferation is not the same but chaotic, according to the value of d_0. For example, when $d_0 = 4$, the proliferation occurs more slowly than the other proliferating cases ($d_0 = 2$ and 3). These results show the initial condition sensitivity still exists even when the proliferation is successful.

7. Difference between photoinduced non-equilibrium phase and high-temperature equilibrium phase

In the light of the progress of experimental and theoretical studies on photoinduced phase transitions, a new but quite basic question has now emerged: namely, how is the photoinduced phase practically different from the high-temperature equilibrium one? As has been mentioned, the photoinduced phase is a non-equilibrium phase, brought about through the multi-stability, or the pseudo-degeneracy of the ground state. However, when this multi-stable situation is realized in our system, a state, similar to the false ground state, is also inferred to appear as an equilibrium phase at high temperatures: that is, through the ordinary thermal phase transition.

In fact, both this photoinduced phase at low temperature and the equilibrium one at high temperature are observed as shown in sections 3 and 5, and these two phases are similar. Thus the aforementioned issue becomes quite serious and significant.

7.1. Photoinduced phase transition in organo-metallic complex crystal

Recent experiments on the photoinduced phenomenon in the organo-metallic complex crystal $[Fe(2\text{-pic})_3]Cl_2 \cdot Et\,OH$ (2-pic = 2-amino-methyl-pyridine) have opened a new prospect in the study of the aforementioned difference. In this crystal, as shown in figure 15, an Fe^{2+} ion and its neighbouring six nitrogen atoms of three 2-pic molecules make a complex, which approximately has an O_h symmetry. As schematically shown by dashed lines in this figure, this metal complex is bonded with other three neighbouring ones through the hydrogens, and these hydrogen bonds result in inter-complex interactions. An Fe^{2+} ion has six electrons in its 3d orbitals (t_{2g}, e_g), and these electrons are in a crystal field, whose symmetry is almost O_h as mentioned before. At absolute zero temperature, these six electrons, being in the three t_{2g} orbitals, become diamagnetic ($S = 0$) as shown in figure 15. This diamagnetic phase has a strong light absorption band at around 2 eV, and the colour of this crystal is deep red. At about 120 K, a first-order phase transition occurs from this diamagnetic phase to a paramagnetic one ($S = 2$), as shown in figure 15, and the colour of the crystal changes from deep red to yellow.

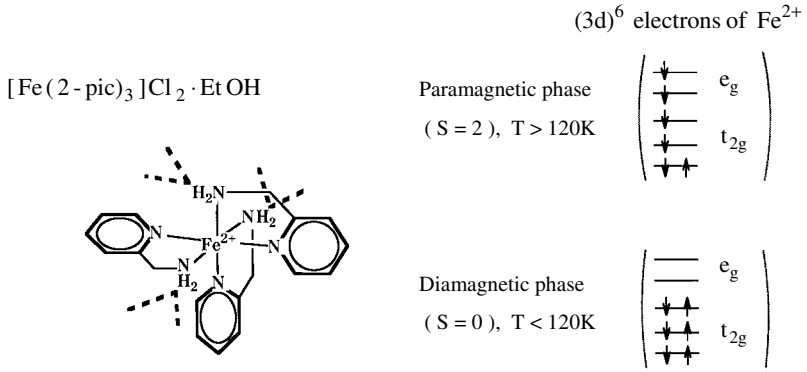

Figure 15. The structure and electronic states of $[Fe(2 - pic)_3]Cl_2 \cdot Et\,OH$.

Ogawa *et al* [20] have recently discovered the photoinduced phase transition in this crystal. Shining 1.8 eV light onto the low-temperature diamagnetic phase of this crystal, they succeeded in generating a macroscopic paramagnetic domain, as shown in figure 16. By this photoinduced phase transition the colour of the crystal changes from the deep red to yellow, which is quite similar to the yellow of the high-temperature paramagnetic phase. They also have found the bi-directional nature of this photoinduced diamagnetic $\leftrightarrow$ paramagnetic transition, and threshold-type behaviour just like in the case of TTF-CA as mentioned in section 3.

In connection with this discovery, very recently, Tayagaki *et al* [21] have also succeeded in observing Raman scattering spectra of these three phases: the low-temperature diamagnetic phase, the high-temperature paramagnetic phase, and the photoinduced paramagnetic phase at low temperature. The resultant three Raman spectra are shown in figure 17. One can clearly see that the photoinduced phase is different from the other two phases, especially in the shaded region, although the other spectral regions are similar to that of the high-temperature paramagnetic phase. Tayagaki *et al* have assigned this difference in the shaded region to come from a new parity violation of the aforementioned O_h symmetry around the 3d orbital.

According to the present status of our experimental study on this organo-metallic complex crystal, however, a new interaction which originates this new parity violation cannot be clarified sufficiently, because this crystal is really complex, as we can easily infer from figure 15.

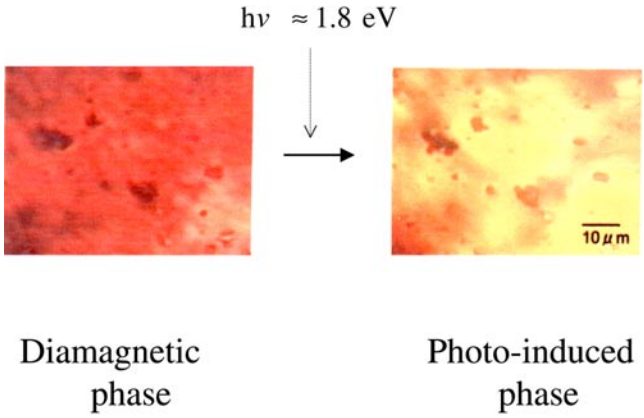

Figure 16. The photoinduced phase transition in $[Fe(2-pic)_3]Cl_2 \cdot Et\,OH$. From Koshihara [20].

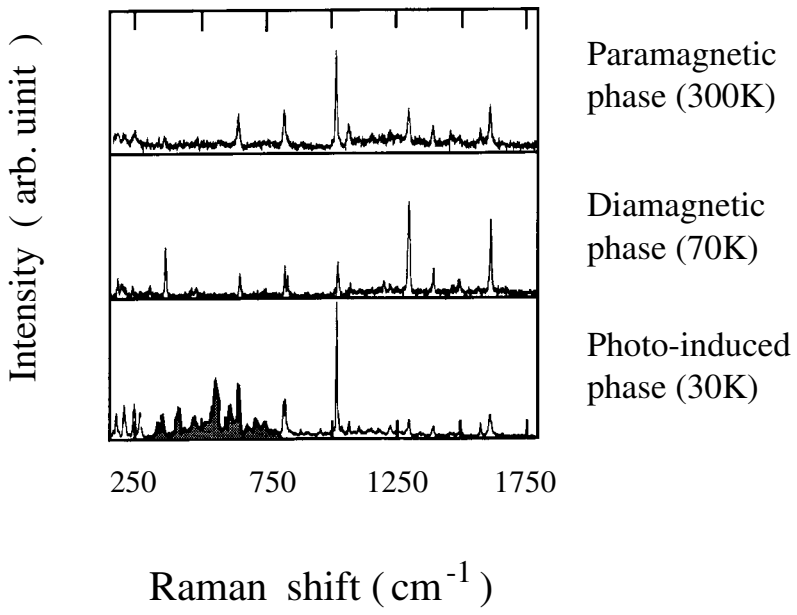

Figure 17. The Raman spectra of $[Fe(2-pic)_3]Cl_2 \cdot Et\,OH$ in the paramagnetic phase (300 K), the diamagnetic phase (70 K) and the photoinduced phase (30 K). The shaded area of the photoinduced phase denotes the eccentric difference from other two spectra. From Tanaka [21].

7.2. Broken symmetry only in photoinduced non-equilibrium phase

It is quite clear that this new broken symmetry (or new parity violation) does not occur in both the two equilibrium phases (the low-temperature diamagnetic phase and the high-temperature paramagnetic phase), but occurs only in the photoinduced non-equilibrium phase at low temperature. This difference between the equilibrium phase and the non-equilibrium one, if once well established conceptionally, will greatly affect our studies of photoinduced phase transitions in other materials. It means that we can discover a new interaction and its resultant broken symmetry through the photoinduced non-equilibrium phase at low temperatures, even

if this new interaction is not clearly observed in any equilibrium phase, such as the true ground-state or high-temperature equilibrium phases.

Here, we should note how to recognize whether a new interaction exists and is operating in a material. Ordinarily, such an interaction (or its resultant broken symmetry) is often neglected or regarded not to exist at all from the beginning, if it is not clearly observed in any equilibrium phases. The aforementioned experimental result [21], however, clearly tells us that this is a prejudice which we have to overcome.

In order to make this point clear, let us now theoretically study a model system which is more simple and standard than the organo-metallic case. Our purpose is to theoretically describe the situation that a new interaction (H_n) appears explicitly only in the low-temperature non-equilibrium phase as a broken symmetry, under the condition that it is almost completely hidden in any other equilibrium phases at low and high temperatures. For this reason, we take a quasi-two-dimensional system composed of N_t lattice sites and N_t electrons, coupled strongly with site-localized phonons. Using this model, we will calculate the CDW-type metal–insulator transition together with the new non-equilibrium phase at low temperatures, from a unified theoretical point of view within the mean field theory. Its Hamiltonian (H_d) is given as

$$H_d = -T_d \sum_{\langle \ell,\ell' \rangle} \sum_{\sigma} C^{+}_{\ell,\sigma} C_{\ell',\sigma} - S_d \sum_{\ell} Q_\ell (n_\ell - 1) + \sum_{\ell} W(Q_\ell) + H_n \qquad (16)$$

$$H_n = U_d \sum_{\ell} n_{\ell,\alpha} N_{\ell,\beta} \qquad (17)$$

where T_d denotes the transfer energy of electron between nearest neighbouring two sites ℓ and ℓ' in a square lattice, and $\langle \ell, \ell' \rangle$ denotes this nearest neighbouring relation. S_d denotes the coupling constant between electrons and a site-localized phonon mode whose coordinate is Q_ℓ. $W(Q_\ell)$ denotes the potential energy of this site-localized phonon, while the kinetic energy of this phonon is neglected, because of the adiabatic approximation. This $W(Q_\ell)$ is assumed to be a triple-well function of Q_ℓ,

$$W(Q_\ell) = (w_1 Q_\ell^2 - w_2 Q_\ell^4 + w_3 Q_\ell^6) \qquad (18)$$

and $w_i (i = 1, 2, 3)$ is the $2i$th expanding coefficient of $W(Q_\ell)$ with respect to Q_ℓ. An anharmonicity is again introduced, to make various equilibrium and non-equilibrium phases of this system locally stable, or to make various phase transitions of this system first-order ones. As for the new interaction H_n, we assume a Hubbard type inter-electron interaction with only a small repulsion U_d.

When the strong coupling and the weak correlation condition ($S_d > T_d > U_d$) is realized, the ground state of this system will be the CDW-type insulator, in which two electrons with up and down spins make a strongly bound singlet pair, and this pair occupy a single site every two sites, along both the x and y axes of this two-dimensional square lattice. Its high-temperature phase will be the ordinary paramagnetic metallic state, although it has a very weak CDW-type order because our model shown in (16) has the complete nesting.

As a typical example to describe this situation, we take following parameter values: $T_d = 0.5$ eV, $S_d = 3$ eV, $U_d = 0.3$ eV, $w_1 = 0.185$ eV, $w_2 = 0.4$ eV, $w_3 = 0.44$ eV, and assume the CDW- and SDW-type broken symmetries with the double period in both x and y directions as

$$\langle n_{\ell,\sigma} \rangle = \tfrac{1}{2} + (-1)^{\ell_x + \ell_y} \delta n_\sigma \qquad Q_\ell = (-1)^{\ell_x + \ell_y} Q_0 \qquad (19)$$

where ℓ_x and ℓ_y are x and y components of ℓ, and other things in (19) are the same as in equation (10), except for Q_0 which denotes the amplitude of CDW-type lattice distortion. Calculated results within the unrestricted Hartree–Fock approximation are shown in figure 18. The transition temperature of system is 221 K as shown in figure 18(a), and our system

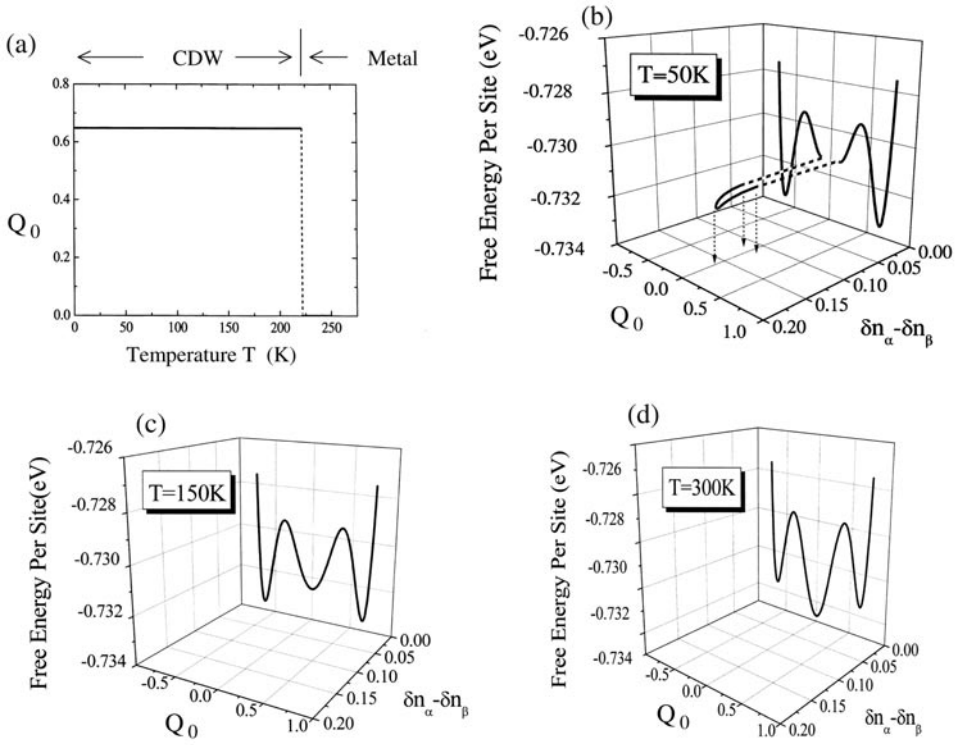

Figure 18. (a) The phase diagram, and Q_0 as a function of temperature T. (b)–(d) Free energies in the two-dimensional space spanned by Q_0 and $\delta n_\alpha - \delta n_\beta$: (b) 50 K, (c) 150 K and (d) 300 K.

discontinuously changes from the CDW state to the metallic one through a first-order phase transition. This first-order nature is due to the anharmonicity in (18).

Let us now focus on the effect of the new interaction H_n. Figures 18(b), (c) and (d) show the calculated free energies as functions of Q_0 and the antiferromagnetic order parameter $\delta n_\alpha - \delta n_\beta$. The figures include both equilibrium and non-equilibrium phases, and they become local minima in this order parameter space spanned by Q_0 and $\delta n_\alpha - \delta n_\beta$. The antiferromagnetic order appears neither in the low-temperature CDW phase nor in the high-temperature metallic one, although the original Hamiltonian H_d does include H_n. As mentioned before, in the CDW state shown in figure 18(c), up- and down-spin electrons make a strongly bound singlet pair through S_d in (16), and this pair occupies a lattice site alternately along the two crystal axes, just as in figure 4(a). This strong singlet pairing kills the antiferromagnetic order, while, in the metallic phase shown in figure 18(d), its high temperature obscures the antiferromagnetic order. Thus, the antiferromagnetic order can appear only as a locally stable non-equilibrium phase at low temperature, as shown in figure 18(b).

Under this circumstance, the new interaction H_n itself is often regarded as non-existent from the outset. However, if this CDW ground state is illuminated by a light at low enough temperature, a CT excitation occurs, and by this excitation, up and down electrons in a lattice site will be separated into two neighbouring lattice sites as an antiferromagnetic pair. This antiferromagnetic pair, once generated by light, will proliferate and will make a non-equilibrium SDW domain just as in figure 4(b). Consequently, the photoinduced phase transition research discloses a new interaction, even if it is completely hidden in all the equilibrium phases.

8. Further problems in photoinduced phase transitions

The history of photoinduced phase transition research is quite young, and there are a number of further problems, which are important but have not been referred to in the preceding sections.

As for the theories of the photoinduced phase transitions, here we have been concerned only with the so-called itinerant models, in which the electrons or the excitons are itinerant from site to site. In this connection, Koshino and Ogawa [22] have developed a unique theory based on a site-localized two-level system (ground and excited states) interacting with other sites ones through a classical spring constant. They term this 'domino theory' since, in this model, a site-localized electronic excitation can proliferate through the spring constant just as in the domino game. This theory successfully describes the photoinduced collective phenomena of the previous organo-metallic complex crystal.

In the previous sections we have been concerned only with the PSPT, which involves some change of the lattice structure. However, there are various other cases, such as photoinduced magnetic phase transitions [23] and the photoinduced superfluid transitions of high-density excitons [24–26], in which phase transitions or order formations occur only in the electronic degree of freedom, without structural change of the lattice. Thus, through the photoinduced phase transition research, we will be able to discover various new phases, with and without structural change.

Acknowledgment

This work is supported by a grant-in-aid of the Japanese ministry of Education, Science and Culture, priority area (B) 'Photoinduced Phase Transitions and their Dynamics'.

References

[1] Ueta M, Kanzaki H, Kobayashi K, Toyozawa Y and Hanamura E 1986 *Excitonic Processes in Solids* (Berlin: Springer) p 203
[2] Nasu K 1997 *Relaxations of Excited States and Photo-Induced Structural Phase Transitions* ed K Nasu (Berlin: Springer) p 6
[3] Kittle C 1996 *Introduction to Solid State Physics* 7th edn (New York: Wiley) p 53
[4] Koshihara S, Takahashi H, Sakai H, Tokura Y and Luty T 1999 *J. Phys. Chem.* B **103** 2592
[5] Suzuki T, Sakamaki T, Tanimura K, Koshihara S and Tokura Y 1999 *Phys. Rev.* B **60** 6191
[6] Thompson J and Stewart H 1986 *Nonlinear Dynamics and Chaos* (New York: Wiley)
[7] Huai P, Zheng H and Nasu K 2000 *J. Phys. Soc. Japan* **69** 1788
[8] Cointe M, Cailleau M, Cailleau H, Toudic B, Toupet L, Heger G, Moussa F, Schweiss P, Kraft K and Karl N 1995 *Phys. Rev.* B **51** 3374
[9] Soos Z 1974 *Ann. Rev. Phys. Chem.* **25** 121
[10] Sakano T and Toyozawa Y 1997 *Relaxations of Excited States and Photo-Induced Structural Phase Transitions* ed K Nasu (Berlin: Springer) p 160
[11] Su W, Schrieffer J and Heeger A 1980 *Phys. Rev.* B **22** 2099
[12] Nagaosa N 1986 *J. Phys. Soc. Japan* **55** 2754
[13] Hayashi H and Nasu K 1985 *Phys. Rev.* B **32** 5295
[14] Katan C, Koenig C and Blochl P 1997 *Solid State Commun.* **102** 589
[15] Jacobsen C and Torrance J 1983 *J. Chem. Phys.* **78** 112
[16] Nasu K 2000 *Electron Conduction in Oxides* ed N Tsuda (Berlin: Springer) p 107
[17] Tomita N and Nasu K 2001 *Phys. Rev.* B **63** 085 107
[18] Mizouchi H and Nasu K 2000 *J. Phys. Soc. Japan* **69** 1543
[19] Mizouchi H and Nasu K 2001 *J. Phys. Soc. Japan* **70** 2175
[20] Ogawa Y, Koshihara S, Koshino K, Ogawa T, Urano C and Takagi H 2000 *Phys. Rev. Lett.* **84** 3181
[21] Tayagaki T and Tanaka K 2001 *Phys. Rev. Lett.* **86** 2886

[22] Koshino K and Ogawa T 1999 *J. Phys. Soc. Japan* **68** 2164
[23] Matsuda K, Machida A, Moritomo Y and Nakamura A 1998 *Phys. Rev.* B **58** R4203
[24] Fortin E, Fafard S and Mysyrowics A 1993 *Phys. Rev. Lett.* **70** 3951
[25] Karasawa T, Mino H and Yamamoto M 2000 *J. Lumin.* **87–89** 174
[26] Inagaki T, Iida T and Aihara M 2000 *Phys. Rev.* B **62** 10 852